Beslier, M.-O., Whitmarsh, R.B., Wallace, P.J., and Girardeau, J. (Eds.)
Proceedings of the Ocean Drilling Program, Scientific Results Volume 173

4. Eocene Calcareous Nannofossil Biostratigraphy and Sediment Accumulation of Turbidite Sequences on the Iberia Abyssal Plain, ODP Sites 1067–1069[1]

Kristeen L. McGonigal[2] and Sherwood W. Wise Jr.[2]

ABSTRACT

Six sites were drilled on the southern Iberia Abyssal Plain during Ocean Drilling Program (ODP) Leg 173. Three holes (1067A, 1068A, and 1069A) recovered Eocene sediments consisting of thinly bedded turbidite deposits with interbedded hemipelagic sediments (Bouma sequence Te) deposited near the calcite compensation depth. The hemipelagic sediments are barren of nannofossils, necessitating the use of the turbidite deposits to erect an Eocene biostratigraphy for these holes. Moderately preserved, diverse assemblages of nannofossils were recovered from silty clays (Bouma sequence Td) and poorly preserved, less diverse assemblages were recovered from sandy/silty clays (Bouma sequence Tc). Hole 1067A has a continuous record of sedimentation (Subzones CP9a–CP14a) and Holes 1068A and 1069A have similar continuous records (Subzones CP9a–CP12a), although all holes contain barren intervals. Holes 1067A, 1068A, 1069A, 900A (ODP Leg 149), and 398D (Deep Sea Drilling Project Leg 47B) display a similar increase in mass accumulation rates in the lowermost middle Eocene. A reliable Eocene biostratigraphy has been erected using nannofossil data from turbidite sequences, allowing for correlation between Iberia Abyssal Plain sites.

[1] McGonigal, K.L., and Wise, S.W., Jr., 2001. Eocene calcareous nannofossil biostratigraphy and sediment accumulation of turbidite sequences on the Iberia Abyssal Plain, ODP Sites 1067–1069. *In* Beslier, M.-O., Whitmarsh, R.B., Wallace, P.J., and Girardeau, J. (Eds.), *Proc. ODP, Sci. Results*, 173, 1–35 [Online]. Available from World Wide Web: <http://www-odp.tamu.edu/publications/173_SR/VOLUME/CHAPTERS/SR173_04.PDF>. [Cited YYYY-MM-DD]
[2] Department of Geological Sciences, Florida State University, Tallahassee FL 32306, USA. Correspondence author: **roessig@gly.fsu.edu**

Initial receipt: 20 October 1999
Acceptance: 30 August 2000
Web publication: 30 April 2001
Ms 173SR-008

INTRODUCTION

The western continental margin of the Iberian peninsula extends from Cape Finisterre in the north to Cape Saint Vincent in the south. The southern Iberia Abyssal Plain (IAP) is bound by a steep continental shelf to the east (Fig. F1), the Vasco da Gama Seamount to the north, and by the Estremadura Spur to the south (Whitmarsh, Beslier, Wallace, et al., 1998). Six sites were drilled during Ocean Drilling Program (ODP) Leg 173 on the West Iberia continental margin to continue the east-west transect across the ocean-continent transition begun by ODP Leg 149. In addition to investigating the mechanisms of thinning and breakup of the continental lithosphere, a key objective of Leg 173 was to investigate the early sedimentary history of the rifted margin (Whitmarsh, Beslier, Wallace, et al., 1998).

Sedimentary sequences overlying structural highs were recovered using the rotary core barrel system at Sites 1065, 1067, 1068, 1069, and 1070. At Holes 1067A, 1068A, and 1069A, we cored continuous middle to lower Eocene upward-darkening turbidite sequences of calcareous siltstone/sandstones, calcareous silty claystones, and claystones (Fig. F2). Pelagic sediments in these holes contain a poor nannofossil record, necessitating the use of nannofossil datums from turbidite sequences to establish a reliable biostratigraphy. Leg 173 sediments were deposited near the calcite compensation depth (CCD) and are similar to sediments recovered during Leg 149 at nearby Site 900 (Shipboard Scientific Party, 1998a, 1998b, 1998c). Site 398 near the Vigo Seamount (Deep Sea Drilling Project [DSDP] Leg 47B) also recovered middle to lower Eocene sediments consisting of fine-grained current and/or turbidite deposits (Sibuet, Ryan, et al., 1979).

Turbidites are generally unfit for the construction of an accurate biostratigraphy because of the large number of reworked nannofossils. Studies of Quaternary turbidites on the Madeira Abyssal Plain (MAP), off the east coast of Africa, however, have shown that an accuracy of 50–500 k.y. can be obtained (Weaver and Thomson, 1993) when constructing a nannofossil biostratigraphy from turbidite deposits. Weaver (1994) used synthetic mixtures of nannofossils and compared them to actual deposits to show that turbidite sediment source bodies are tabular in shape and contain sediment with an age range of 50–500 k.y. Additionally, Weaver and Thomson (1993) were able to show that turbidity flows are only slightly erosive in their transport to the abyssal plain, with less than 12% of the flow being derived from erosion of underlying sediments. This technique has since proven useful in Miocene and Paleogene turbidites on the MAP (Howe and Sblendorio-Levy, 1998), where pelagic interbeds were barren of nannofossils.

The purpose of this study is to document the calcareous nannofossils from Eocene turbidite sediments on the IAP recovered during Leg 173. Additionally, the use of turbidite sequences in constructing a reliable biostratigraphy in Eocene sediments outside of the MAP has been tested. The nannofossil biostratigraphy has been used to construct age-depth plots, to calculate linear sedimentation and mass accumulation rates, and to establish an early–middle Eocene regional correlation between Holes 1067A, 1068A, 1069A, 900A, and 398D.

F1. Location map of the Iberia Abyssal Plain, p. 15.

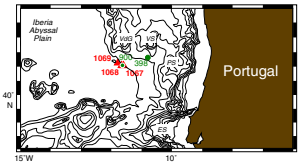

F2. Typical upward-darkening Bouma sequences, p. 16.

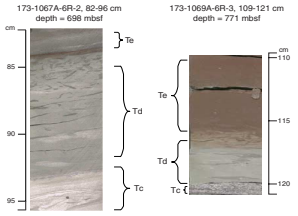

METHODS

Standard nannofossil smear-slide techniques were used to prepare samples. Unprocessed sediment was distributed on a glass coverslip using a mild (<3%) Calgon solution to achieve dispersal between the nannofossils and the clay fraction. Samples were dried and mounted on glass slides using Norland optical adhesive-61 mounting medium. The nannofossil biostratigraphy presented here is based on examination of each sample using a Zeiss photomicroscope III under 500× magnification, using phase-contrast and cross-polarized light. Relative abundance of each nannofossil species, overall preservation of the nannofossil assemblage, and the relative abundance of nannofossils were recorded for each sample using BugWin software (BugWare, Inc.).

Range charts presented in Tables **T1, T3,** and **T5** were created using these measurements. Individual species abundance are represented by the following abbreviations:

V = very abundant; >100 specimens per 10 fields of view (FOV);
A = abundant; 11–100 specimens per 10 FOV
C = common; 6–10 specimen per 10 FOV;
F = few; 1–5 specimen per 10 FOV; and
R = rare; 1 specimen per >10 FOV.

The same definitions were used for estimations of total abundance of each sample, with the additional definition of "B" (B = barren of nannofossils). Preservation of the calcareous nannofossil assemblage was determined as follows:

G = good; individual specimens exhibit little or no dissolution or overgrowth; diagnostic characteristics are preserved and nearly all of the specimens can be identified;
M = moderate; individual specimens show evidence of dissolution or overgrowth; some specimens cannot be identified to the species level; and
P = poor; individual specimens exhibit considerable dissolution or overgrowth; many specimens cannot be identified to the species level.

For scanning electron microscope study, samples were prepared following the settling technique of de Kaenel and Bergen (1996), mounted on a glass coverslip taped to a specimen stub, and coated with a thin film of gold-platinum alloy in a vacuum coater.

Calcareous nannofossil species considered in this paper are listed in **"Appendix,"** p. 13, where they are arranged alphabetically by generic epithets. Bibliographic references for these taxa can be found in Perch-Nielsen (1985) and Bown (1998).

ZONATION

A combination of the nannofossil zonal schemes of Martini (1971) and Okada and Bukry (1980) is used for Leg 173 Eocene sediments (Fig. **F3**). All early and middle Eocene zonal markers and boundaries of Martini (1971) or Okada and Bukry (1980) except for *Coccolithus crassus* and *Rhabdosphaera gladius* can be recognized, although some of the zonal

F3. Eocene calcareous nannofossil biostratigraphic datums, p. 17.

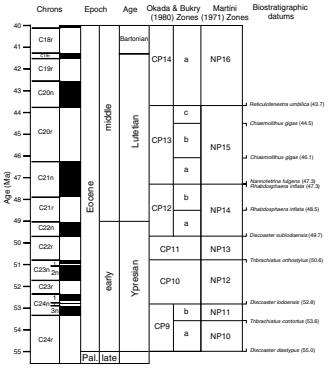

markers are rare. All early and middle Eocene zones from NP10/CP9a through NP16/CP14a are present.

The Paleocene/Eocene boundary is defined in this study by the first occurrence (FO) of *Discoaster diastypus,* which marks the CP8/CP9 boundary in Okada and Bukry's (1980) zonal scheme. The FO of *Tribrachiatus bramlettei,* used by Martini to define this boundary (NP9/NP10), is difficult to distinguish in the lower Eocene at these sites because of poor preservation and was not used. The FO of *Discoaster sublodoensis* determines the early/middle Eocene boundary (NP13/NP14 or CP11/CP12a). Although preservation of this delicate nannofossil is poor, its distinctive form is easily identified.

ACCUMULATION RATES

Linear sedimentation rate (LSR) and mass accumulation rate (MAR) are calculated based on FO and LO (last occurrence) of biostratigraphically important nannofossils. Key nannofossil datums and absolute ages (Berggren et al., 1995) used to determine LSR and MAR are listed in Figure **F3.** MAR is calculated after Van Andel, et al. (1975) and uses average values for wet bulk density and porosity. MAR was calculated using the following equation:

$$\mathrm{MAR} = T[BD - (P \times \mathrm{WD})]/\mathrm{t},$$

where BD = wet bulk density (in grams per cubic centimeter), P = porosity (in weight percent), WD = seawater density (WD = 1.025 g/cm^3), and T is the thickness of sediment that accumulated over time t (t = 10^6 yr). Limited numbers of measurements are available from multisensor track data taken by the Shipboard Scientific Parties of Legs 173 (1998a, 1998b, 1998c), 149 (1994), and 47B (Williams and Mountain, 1979) and can be found in the appropriate chapters of each *Initial Reports* volume.

RESULTS

Hole 1067A Summary

Coring of Hole 1067A (40°40.950′N, 11°35.750′W, water depth = 5020.9 m) began 648 meters below seafloor (mbsf), and Eocene sediments were recognized between Samples 173-1067A-1R-1, 34–36 cm, and 13R-1, 30–31 cm (Fig. **F1**). The stratigraphic distribution of nannofossils is indicated in Table **T1.** Key biohorizons are listed in Table **T2,** along with their sample interval and average depth. These sediments consist mainly of grayish green calcareous siltstones, grayish green nannofossil claystones, and moderate brown claystones. Calcareous nannofossils are abundant in most samples. Their preservation is generally good to moderate, grading to poor downhole, and is facies controlled.

Samples 173-1067A-1R-1, 34–36 cm, through 1R-CC, 21–23 cm, are middle Eocene in age and belong to the *Discoaster bifax* Zone (CP14a/NP16), based on the FO of *D. bifax*. *Reticulofenestra umbilica* is also used by Okada and Bukry (1980) to mark the beginning of this zone. This marker is not employed in this study, as *R. umbilica* appears sporadically and *Reticulofenestra samodurovii* has been shown to grade into *R. umbilica*, with size being conventionally used to separate the two species

T1. Stratigraphic distribution of calcareous nannofossil taxa, Hole 1067A, p. 21.

T2. Summary of key nannofossil biohorizons, Hole 1067A, p. 22.

(Perch-Nielsen, 1985). Common assemblage nannofossils in this zone are *Chiasmolithus solitus, Coccolithus pelagicus, Discoaster barbadiensis, Girgisia gammation, Reticulofenestra dictyoda, R. samodurovii,* and *Sphenolithus moriformis*. The nannofossils are abundant and well to moderately preserved.

The *Nannotetrina quadrata* Zone (CP13/NP15) of Okada and Bukry (1980) is broken into three subzones. The *Birkelundia staurion* "gap" Subzone (CP13c) is demarcated by the LO of *Chiasmolithus gigas* and the absence of *D. bifax* and *R. umbilica*. This subzone occurs from Samples 173-1067A-2R-1, 121–122 cm, through 2R-CC, 13–16 cm. This subzone contains common nannofossils represented by *Coccolithus formosus, C. pelagicus, G. gammation, R. dictyoda, Sphenolithus furcatolithoides, S. moriformis,* and *Sphenolithus radians,* which are moderately preserved. The *C. gigas* Subzone (CP13b) occurs from Samples 173-1067A-3R-1, 34–35 cm, to 5R-3, 8–9 cm, and is marked by the presence of *C. gigas*. This subzone contains several poorly preserved and barren intervals that occur in siltstone and claystone layers. Sample 173-1067A-5R-3, 48–49 cm, is the first sample in the *Discoaster strictus* Subzone (CP13a) of Okada and Bukry (1980). This interval is marked by the absence of *C. gigas* and the FO of *Nannotetrina fulgens* (*N. quadrata* of other authors). The FO of *N. fulgens* is difficult to pinpoint because of the overgrowth of most specimens. Some authors use the FO of the *Nannotetrina* genus to mark the beginning of Subzone CP13a (Perch-Nielsen, 1985), but this genus appears ~6 m below the LO of *Rhabdosphaera inflata* in Hole 1067A. This study uses the last appearance of few specimens of *R. inflata* to mark the bottom of Subzone CP13a. Rare *R. inflata* specimens observed above Sample 173-1067A-7R-2, 32–33 cm, are considered reworked.

The *Rhabdosphaera inflata* Subzone (CP12b) begins with Sample 173-1067A-7R-3, 32–33 cm, and continues through Sample 173-1067A-8R-4, 30–31 cm. This subzone is marked by the occurrence of *R. inflata*. Nannofossils are moderately preserved throughout this interval and are represented by *C. pelagicus, Discoaster barbadensis, Discoaster deflandrei, Discoaster tanii, R. dictyoda, S. moriformis,* and *Zygrhablithus bijugatus*. The *Discoaster kuepperi* Subzone (CP12a) is marked by the absence of *R. inflata* and the presence of *D. sublodoensis* and begins with Sample 173-1067A-8R-CC, 23–25 cm. Nannofossils are commonly present and poorly preserved throughout this interval, which is characterized by the presence of *C. pelagicus, D. barbadensis, R. dictyoda,* and *Z. bijugatus*. The middle/early Eocene boundary is placed between Samples 173-1067A-9R-3, 37–38 cm, and 9R-3, 121–122 cm, based on the FO of *D. sublodoensis*.

The *Discoaster lodoensis* Zone (CP11/NP13) extends from Sample 173-1067A-9R-3, 121–122 cm, through 11R-1, 36–37 cm. The boundary between Zones CP11/CP10 (NP13/NP12) in this study is based on the LO of *Tribrachiatus orthostylus,* as *C. crassus* cannot be identified because of poor preservation. *C. pelagicus, D. barbadensis,* and *D. lodoensis* dominate this moderately preserved assemblage.

The *T. orthostylus* Zone (CP10/NP12) begins with Sample 173-1067A-11R-1, 119–120 cm, and continues through Sample 173-1067A-11R-2, 121–122 cm. This short interval contains moderately preserved common nannofossils represented by *C. pelagicus, S. moriformis,* and *T. orthostylus*.

Sample 173-1067A-11R-3, 40–41 cm, begins the *Discoaster binodosus* Subzone (CP9b/NP11). This "gap" zone is marked by the absence of *D. lodoensis* and *Tribrachiatus contortus*. Nannofossils are common and moderately to poorly preserved, and there are two barren intervals.

Common nannofossils in this interval are *C. pelagicus, D. barbadensis, D. deflandrei, S. moriformis,* and *T. orthostylus*. Sample 173-1067A-12R-CC, 10–12 cm, contains the first *T. orthostylus* and no *T. contortus* and is the last sample in Subzone CP9b.

Subzone CP9a (Okada and Bukry, 1980) is marked by the presence of *D. diastypus* and *T. contortus*, and the corresponding Zone NP10 (Martini, 1971) is marked by the FO of *T. bramlettei*. These events are not synchronous (Berggren et al., 1995), all occurring slightly before the currently drawn Paleocene/Eocene boundary. Because of preservational constraints and the scarcity of both *Tribrachiatus* markers, this study bases the beginning of the Eocene epoch and the bottom of Zones CP9a/NP10 on the FO of *D. diastypus,* even though a solid magnetochronologic age for the FO of *D. diastypus* has not been recorded (Berggren et al., 1995). Ladner and Wise (**Chap. 5,** this volume) have also adopted this definition. The lowermost Eocene zone is represented by three samples from Samples 173-1067A-12R-CC, 25–27 cm, to 13R-1, 30–31 cm. Nannofossils are abundant and moderately preserved, although one interval of grayish brown clay is barren. The nannofossil assemblage shows poor diversity, being dominated by *D. diastypus, C. pelagicus,* and *S. moriformis*.

Hole 1068A Summary

Coring of Hole 1068A (40°40.955′N, 11°36.720′W, water depth = 5043.9 m) began at 711.3 mbsf (Fig. **F1**) and contains Eocene sediments between Samples 173-1068A-1R-1, 35–36 cm, and 8R-3, 7–8 cm. Calcareous nannofossils are abundant and moderately preserved throughout the grayish green calcareous siltstones, light gray-green nannofossil chalks, and greenish gray calcareous claystones of this interval and are listed in Table **T3.** Moderately to poorly preserved calcareous nannofossils are found in the moderately brown claystones and greenish gray calcareous sandy siltstones, which are occasionally barren of calcareous nannofossils. Key biohorizons, their sample interval, and their average depths are listed in Table **T4.**

T3. Stratigraphic distribution of calcareous nannofossil taxa, Hole 1068A, p. 23.

T4. Summary of key nannofossil biohorizons, Hole 1068A, p. 24.

Sample 173-1068A-1R-1, 35–36 cm, is considered the first sample in the middle Eocene *D. sublodoensis* Zone (CP12/NP14). Okada and Bukry (1980) broke this zone into two subzones (CP12a and CP12b) based on the FO of *R. inflata*. Based on the occurrence of *R. inflata,* Samples 173-1068A-1R-1, 35–36 cm, through 1R-6, 36–37 cm, represent the *R. inflata* Subzone CP12b. Samples 173-1068A-1R-CC through 5R-2, 35–36 cm, represent the *D. kuepperi* Subzone CP12a, based on the FO of *D. sublodoensis* and the absence of *R. inflata*. The nannofossil assemblages are moderately well preserved and are dominated by *C. formosus, C. pelagicus, D. barbadensis, D. deflandrei, R. dictyoda, S. moriformis,* and *Z. bijugatus*. The middle/lower Eocene boundary is placed between Sample 173-1068A-5R-1, 121–122 cm, and 5R-2, 35–36 cm, based on the FO of *D. sublodoensis*. The *D. lodoensis* "gap" Zone (CP11/NP13) begins with Sample 173-1068A-5R-2, 35–36 cm, based on the absence of *D. sublodoensis* and *T. orthostylus*. The FO of *C. crassus* could not be determined in these samples because of overgrowth and dissolution.

Sample 173-1068A-6R-3, 121–122 cm, marks the beginning of the *T. orthostylus* Zone (CP10/NP12) based on the presence of *T. orthostylus*. This zone is represented by five samples, three of which are barren claystones.

Sample 173-1068A-6R-6, 38–39 cm, begins the *D. binodosus* "gap" Zone (NP11/CP9b), based on the absence of *D. lodoensis* and *T. contor-*

tus. The nannofossil assemblage is moderately well preserved and dominated by *C. formosus, C. pelagicus, D. barbadensis, D. kuepperi, T. orthostylus,* and *Z. bijugatus*.

The *T. contortus* Zone (CP9a/NP10) extends from Sample 173-1068A-6R-CC, 23–25 cm, through 8R-3, 7–8 cm, based on the presence of *D. diastypus*. The FO of *T. bramlettei* or *T. contortus* did not prove to be reliable markers because they are commonly overgrown and difficult to separate from *Rhomboaster cuspis* (Wei and Zhong, 1996). The nannofossil assemblage is poorly preserved to barren in sandstones and claystones of this zone, which is dominated by *C. pelagicus, D. barbadensis, D. diastypus, D. multiradiatus, Toweius magnicrassus, T. orthostylus,* and *Z. bijugatus*. The Paleocene/Eocene boundary is drawn between Samples 173-1068A-8R-3, 7–8 cm, and 8R-4, 44–45 cm, based on the FO of *D. diastypus*.

Hole 1069A Summary

Coring of Hole 1069A (40°42.612′N, 11°46.633′W, water depth = 5074.8 m) began at 718.8 mbsf and recovered 147 m of sediment overlying metasedimentary rocks (Fig. **F1**). Eocene sediments were recognized in Samples 173-1069A-1R-1, 3–5 cm, through 7R-4, 61-63 cm, and are listed in Table **T5.** Calcareous nannofossils are abundant and moderately well preserved in these sediments. Preservation again is facies controlled, with poor preservation of nannofossils in the moderately brown clays and improved preservation in the greenish gray nannofossil claystones and greenish gray sandy siltstones. Preservation also declines downsection. Table **T6** lists sample intervals and average depths of key nannofossil biohorizons.

T5. Stratigraphic distribution of calcareous nannofossil taxa, Hole 1069A, p. 25.

T6. Summary of key nannofossil biohorizons, Hole 1069A, p. 26.

Sample 173-1069A-1R-1, 3–5 cm, is considered the first sample in the middle Eocene based on the occurrence of *R. inflata* (Subzone CP12b). The interval between Samples 173-1069A-1R-CC and 5R-2, 29–30 cm, contains no *R. inflata* and is assigned to the *D. sublodoensis* (NP14) Zone or the *D. kuepperi* Subzone (CP12a). *C. pelagicus, D. barbadensis, D. kuepperi, D. tanii, G. gammation, R. dictyoda, S. radians,* and *Z. bijugatus* dominate the assemblage. The boundary between the middle and early Eocene is placed between Samples 173-1069A-5R-2, 29–30 cm, and 5R-CC, 1–2 cm.

The early Eocene *D. lodoensis* Zone (CP11/NP13) extends from Samples 173-1069A-5R-2-CC, 1–2 cm, to 5R-2-CC, 14–17 cm. Difficulties exist in discerning the CP11 *D. lodoensis* Zone defined by Okada and Bukry (1980) by the FO of *C. crassus,* which could not be determined in these samples because of overgrowth and dissolution of the nannofossils. Instead, the datums marking the NP13 "gap" Zone of Martini (1971), defined by the LO of *T. orthostylus* and FO of *D. sublodoensis,* were used.

Sample 173-1069A-6R-1, 4–5 cm, is the first sample of the *T. orthostylus* Zone (CP10/NP12), based on the FO of *D. lodoensis*. The assemblage is dominated by *C. formosus, C. pelagicus, D. barbadensis, D. lodoensis, S. radians, T. orthostylus,* and *Z. bijugatus*.

Sample 173-1069A-6R-5, 87–88 cm, is the first sample of the *D. binodosus* "gap" Zone (CP9b/NP11), based on the absence of *T. contortus* and *D. lodoensis*. Preservation of nannofossil assemblages in this zone shows a rapid change to poor preservation compared with previous zones with moderate preservation. The assemblage is dominated by *C. pelagicus, D. barbadensis, D. binodosus, D. diastypus, T. bramlettei,* and *T. orthostylus*.

Sample 173-1069A-7R-1, 147–150 cm, is the first sample belonging to the *T. contortus* Zone (CP9a/NP10), based on the FO of *D. diastypus*. No nannofossils were found from Samples 173-1069A-7R-2, 33–35 cm, through 7R-4, 61–63 cm. These samples are considered to be early Eocene in age, based on the absence of *D. diastypus, T. bramlettei,* and *T. contortus* in Sample 173-1069A-7R-5, 1–3 cm, marking the beginning of upper Paleocene sediments (Ladner and Wise, **Chap. 5,** this volume).

Hole 900A Summary

The thickest, most complete Eocene section recovered during ODP Leg 149 (Fig. **F1**) was at Hole 900A (46°40.994′N, 11°36.252′W, water depth = 5036.8 m). The dominant lithology in the Eocene section is upward-darkening turbidite sequences (Shipboard Scientific Party, 1994). The Eocene calcareous biostratigraphy of Hole 900A was previously described by Liu (1996). Her original smear slides have been reexamined using the species and boundary definitions of this study to facilitate a comparison with the zonal schemes established for Holes 1067A, 1068A, and 1069A. Early to middle Eocene sediments complimentary to those drilled at Leg 173 sites were found in Samples 149-900A-64R-2, 100–101 cm, to 77R-3, 3–4 cm. Calcareous nannofossils are abundant and moderately to poorly preserved in the hemipelagic and pelagic sediments deposited above the CCD. Minor modifications to Liu's (1996) biostratigraphy are summarized in Table **T7,** which lists sample intervals and average depths of key nannofossil biohorizons, as defined in this study.

Hole 398D Summary

During DSDP Leg 47B, one site was drilled (40°57.6′N, 10°43.1′W) on the southern flank of the Vigo Seamount (Fig. **F1**) in 1976. The original nannofossil biostratigraphy was completed by Blechschmidt (1979), who loosely applied the zonation of Martini (1971). Samples located between Blechschmidt-assigned zonal boundaries were analyzed to further constrain these boundaries and to look for key Okada and Bukry (1980) and Martini (1971) markers that were not originally recorded. Samples 47B-398D-35R-7, 30–31 cm, to 23R-1, 25–26 cm, contain lower to middle Eocene sediments complementary to those recovered in Holes 1067A, 1068A, and 1069A. Calcareous nannofossils were abundant and moderately preserved throughout this interval. *C. gigas* was found in only one sample, and Subzone CP13b could not be identified. Refinement of Blechschmidt's biostratigraphy is summarized in Table **T8,** which lists sample intervals and average depths of key nannofossil biohorizons.

Stratigraphic correlations between Holes 1067A, 1068A, 1069A, 900A, and 398D are presented in Figure **F4.** Zonal boundary lines are drawn on the FOs and LOs of key biohorizons (Fig. **F3**).

LINEAR SEDIMENTATION RATES

LSRs were calculated for each site and plotted with visual best-fit lines in Figure **F5.** Sedimentation rates for Hole 1067A are based on nine nannofossil age estimates (Table **T2**). Sedimentation rates vary from ~5.5–14.4 m/m.y., with a possible hiatus during the CP10 *T. orthostylus* Zone. Hole 1068A LSRs are based on six nannofossil age estimates

T7. Summary of key nannofossil biohorizons, Hole 900A, p. 27.

T8. Summary of key nannofossil biohorizons, Hole 398D, p. 28.

F4. Eocene correlation among Legs 173, 149, and 47B, p. 18.

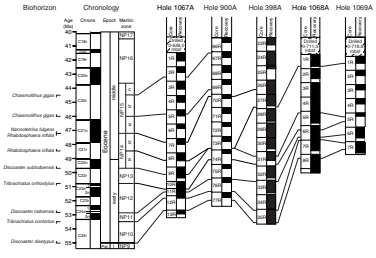

F5. Age-depth plot, p. 19.

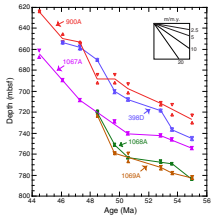

(Table T4) and range from 20 to a low of 2.6 m/m.y. during the CP10 *T. orthostylus* Zone. Six Eocene nannofossil age estimates (Table T6) were used to calculate LSRs for Hole 1069A. Rates vary from 3.0 to 30.0 m/m.y. The CP10/CP11 boundary is constrained only to a broad 7-m interval because of poor recovery (Shipboard Scientific Party, 1998c) in Core 173-1069A-5R (~22% recovery), making it difficult to determine if low sedimentation also prevailed during the *T. orthostylus* Zone (CP10) at Hole 1069A. Hole 900A LSRs are based on eight nannofossil age estimates and range from 3.8 to 28.6 m/m.y. A condensed section/hiatus during the *D. kuepperi* CP12a Subzone is based on the co–first occurrence of *R. inflata* and *D. sublodoensis*. These events should occur 1.2 m.y. apart, although this boundary is broadly constrained to a 7.5-m interval. Other sites studied on the IAP have high sedimentation rates through this interval, and erosion at Site 900, which sits atop a structural high, may explain the difference in sedimentation pattern at Site 900. Sedimentation rates vary from 4.0 to 25.8 m/m.y. at Hole 398D. Site 398 is in close proximity to the Vigo Seamount, and sediments were deposited above the CCD, contributing to differences in sedimentation patterns compared to other IAP sites. Nannofossil age estimates (Fig. F3) are taken from Berggren et al. (1995).

MASS ACCUMULATION RATES

MARs were determined for each site using physical properties data and calculated LSRs. Measurements were averaged through each interval because of poor core recovery and limited shipboard measurements. MARs for Hole 1067A were calculated from 50 physical properties measurements (Fig. F6); 66 physical properties measurements were used for Hole 1068A MARs; 40 physical properties measurements were used for Hole 1069A MARs; 57 physical properties measurements were used for Hole 900A MARs; and 40 physical properties measurements were used for Hole 398D MARs. The physical properties average values used to create Figure F6 are listed in Table T9. Hole 1067A shows decreasing MARs from the middle Eocene to the lower middle Eocene (from 0.2 to 3.5 g/cm²/k.y.). MARs increase in the uppermost lower Eocene (2.3 g/cm²/k.y.), drop off to a hiatus in the upper lower Eocene (<0.2 g/cm²/k.y.), and increase (1.1 g/cm²/k.y.) in the lower Eocene. Holes 1068A, 1069A, 900A, and 398D have similar MAR patterns with a peak (>5.0 g/cm²/k.y.) in the lower middle Eocene, a drop (<2.0 g/cm²/k.y.) in the middle lower Eocene, and a variable increase (1.1–4.1 g/cm²/k.y.) during the lower lower Eocene. The increase in MARs seen at the lower/middle Eocene boundary indicates that sedimentation was greater than subsidence in the rift basin and that turbidity flows were depositing more of their sediments on the basement blocks (structural highs). Overall, the sediments on the IAP show similar MAR patterns with minor variations resulting from increasing distance from sediment source (Hole 1069A) or location on a structural high (Hole 900A).

DISCUSSION

A lower to middle Eocene zonation based on materials from a turbidite-dominated region has provided a detailed nannofossil biostratigraphy and correlation between the Eocene sections of Holes 1067A, 1068A, 1069A, 900A, and 398D (Fig. F4). Eocene sediments recovered at

F6. Mass accumulation rates, p. 20.

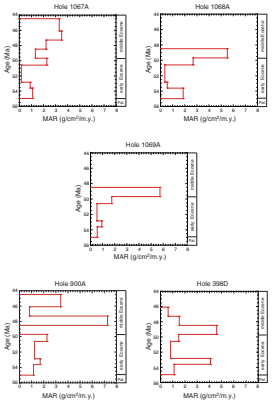

T9. Physical properties data average values used to calculate mass accumulation rates, p. 29.

these sites represent Bouma sequences Tc, Td, and Te (Shipboard Scientific Party, 1979, 1994, 1998a, 1998b, 1998c). These sequences are typical of turbidite sedimentation at distal areas of the lower fan (Walker, 1984). Moderately preserved nannofossil assemblages were recovered from Bouma sequence Td, and poorly preserved or barren assemblages were recovered from Bouma sequences Tc and Te (Fig. **F2**).

All sites examined display a similar overall pattern of mass accumulation through the Eocene. Hole 1067A is located on the continental rise side of a structural high (Fig. **F1**) and has MARs <4.0 g/cm²/k.y. Holes 1068A and 1069A display similar sediment accumulation rates through the Eocene, peaking in the lower middle Eocene (Fig. **F6**) with MARs of ~6 g/cm²/k.y. This is expected, as both sites are on the IAP side of a structural high (Shipboard Scientific Party, 1998a). MARs at Site 900A reveal a hiatus followed by a large increase to 7.3 g/cm²/k.y. that is not evident at other sites. This interval is poorly constrained by the nannofossil biostratigraphy and differences are possibly due to erosion at this site. All sites had very low (<2 g/cm²/k.y.) MARs during the late early Eocene while the basin was still being infilled. A rapid increase in MARs at the lower/middle Eocene boundary indicates that increasing amounts of turbidite sediments were being deposited on the basement blocks as basin infilling progressed. Overall, these low MARs on the IAP are consistent with the observation that this margin has only a thin sediment covering (Whitmarsh, Beslier, Wallace, et al., 1998).

The results of this study support the use of nannofossil biostratigraphy in abyssal plain environments dominated by turbidite deposition. Despite the fact that pelagic sediments were deposited below the CCD and were thus barren of nannofossils, a reliable, consistent Eocene biostratigraphy was constructed based on nannofossils recovered from turbidite sequences. These results have been confirmed by an independent magnetostratigraphic study of these same cores (Zhao et al., **Chap. 11,** this volume).

ACKNOWLEDGMENTS

The first author wishes to thank Drs. S.W. Wise and T.R. Janecek for helpful comments and reviews on early drafts of this paper, which was submitted in partial fulfillment of requirements for a master's degree in geology at Florida State University. We also thank Drs. Richard W. Howe and Alyssa Peleo-Alampay for external review of the final draft. Samples were provided by NSF through ODP. This study was supported by USSAC funds to S.W. Wise. Laboratory facilities were provided by NSF grant no. DPP 94-22893.

REFERENCES

Berggren, W.A., Kent, D.V., Swisher, C.C., III, and Aubry, M.-P., 1995. A revised Cenozoic geochronology and chronostratigraphy. *In* Berggren, W.A., Kent, D.V., Aubry, M.-P., and Hardenbol, J. (Eds.), *Geochronology, Time Scales and Global Stratigraphic Correlation*. Spec. Publ.—Soc. Econ. Paleontol. Mineral. (Soc. Sediment. Geol.), 54:129–212.

Blechschmidt, G., 1979. Biostratigraphy of calcareous nannofossils: Leg 47B, Deep Sea Drilling Project. *In* von Rad, U., Ryan, W.B.F., et al., *Init. Repts. DSDP,* 47 (Pt. 1): Washington (U.S. Govt. Printing Office), 327–360.

Bown, P.R. (Ed.), 1998. *Calcareous Nannofossil Biostratigraphy:* London (Chapman-Hall).

de Kaenel, E., and Bergen, J.A., 1996. Mesozoic calcareous nannofossil biostratigraphy from Sites 897, 899, and 901, Iberia Abyssal Plain: new biostratigraphic evidence. *In* Whitmarsh, R.B., Sawyer, D.S., Klaus, A., and Masson, D.G. (Eds.), *Proc. ODP, Sci. Results,* 149: College Station, TX (Ocean Drilling Program), 27–59.

Howe, R.W., and Sblendorio-Levy, J., 1998. Calcareous nannofossil biostratigraphy and sediment accumulation of turbidite sequences on the Madeira Abyssal Plain, Sites 950–952. *In* Weaver, P.P.E., Schmincke, H.-U., Firth, J.V., and Duffield, W. (Eds.), *Proc. ODP, Sci. Results,* 157: College Station, TX (Ocean Drilling Program), 501–520.

Liu, L., 1996. Eocene calcareous nannofossils from the Iberia Abyssal Plain. *In* Whitmarsh, R.B., Sawyer, D.S., Klaus, A., and Masson, D.G. (Eds.), *Proc. ODP, Sci. Results,* 149: College Station, TX (Ocean Drilling Program), 61–78.

Martini, E., 1971. Standard Tertiary and Quaternary calcareous nannoplankton zonation. *In* Farinacci, A. (Ed.), *Proc. 2nd Int. Conf. Planktonic Microfossils Roma:* Rome (Ed. Tecnosci.), 2:739–785.

Okada, H., and Bukry, D., 1980. Supplementary modification and introduction of code numbers to the low-latitude coccolith biostratigraphic zonation (Bukry, 1973; 1975). *Mar. Micropaleontol.,* 5:321–325.

Perch-Nielsen, K., 1985. Cenozoic calcareous nannofossils. *In* Bolli, H.M., Saunders, J.B., and Perch-Nielsen, K. (Eds.), *Plankton Stratigraphy:* Cambridge (Cambridge Univ. Press), 427–554.

Shipboard Scientific Party, 1979. Site 398D. *In* Sibuet, J.-C., Ryan, W.B.F., et al., *Init. Repts. DSDP,* 47 (Pt. 2): Washington (U.S. Govt. Printing Office), 327–360.

————, 1994. Site 900. *In* Sawyer, D.S., Whitmarsh, R.B., Klaus, A., et al., *Proc. ODP, Init. Repts.,* 149: College Station, TX (Ocean Drilling Program), 211–262.

————, 1998a. Site 1067. *In* Whitmarsh, R.B., Beslier, M.-O., Wallace, P.J., et al., Proc. ODP, Init. Repts., 173: College Station, TX (Ocean Drilling Program), 107–161.

————, 1998b. Site 1068. *In* Whitmarsh, R.B., Beslier, M.-O., Wallace, P.J., et al., *Proc. ODP, Init. Repts.,* 173: College Station, TX (Ocean Drilling Program), 163–218.

————, 1998c. Site 1069. *In* Whitmarsh, R.B., Beslier, M.-O., Wallace, P.J., et al., *Proc.ODP, Init. Repts.,* 173: College Station, TX (Ocean Drilling Program), 219–263.

Sibuet, J.-C., Ryan, W.B.F., et al., 1979. *Init. Repts. DSDP,* 47 (Pt. 2): Washington (U.S. Govt. Printing Office).

van Andel, T.H., Heath, G.R., and Moore, T.C., Jr., 1975. Cenozoic history and paleoceanography of the central equatorial Pacific Ocean: a regional synthesis of Deep Sea Drilling Project data. *Mem.—Geol. Soc. Am.,* 143.

Walker, R.G., 1984. Turbidites and associated coarse-grained clastic deposits. *In* Walker, R.G. (Ed.), *Facies Models* (2nd ed.). Geol. Assoc. Can., Geosci. Reprint Ser., 1:171–188.

Weaver, P.P.E., 1994. Determination of turbidity current erosional characteristics from reworked coccolith assemblages, Canary Basin, North-east Atlantic. *Sedimentology,* 41:1025–1038.

Weaver, P.P.E., and Thomson, J., 1993. Calculation erosion by deep-sea turbidity currents during initiation and flow. *Nature,* 364:136–138.

Wei, W., and Zhong, S., 1996. Taxonomy and magnetobiochronology of *Tribrachiatus* and *Rhomboaster,* two genera of calcareous nannofossils. *J. Paleontol.,* 70:7–22.

Whitmarsh, R.B., Beslier, M.-O., Wallace, P.J., et al., 1998. *Proc. ODP, Init. Repts.,* 173: College Station, TX (Ocean Drilling Program).

Williams, C.A., Mountain, G., 1979. Aspects of physical properties measurements, Leg 47, Sites 397 and 398. *In* Sibuet, J.-C., Ryan, W.B.F., et al., *Init. Repts. DSDP,* 47 (Pt. 2): Washington (U.S. Govt. Printing Office), 585–598.

APPENDIX

Eocene Calcareous Nannofossil Species Considered in this Report

Birkelundia staurion (Bramlette and Sullivan, 1961) Perch-Nielsen (1971)
Blackites spinosus (Deflandré and Fert, 1954) Hay and Towe (1962)
Braarudosphaera bigelowii (Bran and Braarud, 1935) Deflandré (1947)
Braarudosphaera discula Bramlette and Riedel (1954)
Campylosphaera dela (Bramlette and Sullivan, 1961) Hay and Mohler (1967)
Chiasmolithus altus Bukry and Percival (1971)
Chiasmolithus bidens (Bramlette and Sullivan, 1961) Hay and Mohler (1967)
Chiasmolithus consuetus (Bramlette and Sullivan, 1961) Hay and Mohler (1967)
Chiasmolithus expansus (Bramlette and Sullivan, 1961) Gartner (1970)
Chiasmolithus gigas (Bramlette and Sullivan, 1961) Radomski (1968)
Chiasmolithus grandis (Bramlette and Sullivan, 1961) Radomski (1968)
Chiasmolithus modestus Perch-Nielsen (1971)
Chiasmolithus omaruensis (Deflandré, 1954) Hay, Mohler and Wade (1966)
Chiasmolithus solitus (Bramlette and Sullivan, 1961) Locker (1968)
Chiasmolithus titus Gartner (1970)
Clausicoccus subdistichus (Deflandré and Fert, 1954) Prins (1979)
Coccolithus eopelagicus (Bramlette and Riedel, 1954) Bramlette and Sullivan, (1961)
Coccolithus formosus (Kamptner, 1963) Wise (1973)
Coccolithus pelagicus (Wallich, 1877) Schiller (1930)
Coronocyclus nitescens (Kamptner, 1963) Bramlette and Wilcoxon (1967)
Coronocyclus prionion (Deflandré and Fert, 1954) Stradner in Stradner and Edwards (1968)
Cruciplacolithus tenuis (Stradner, 1961) Hay and Mohler in Hay et al. (1967)
Discoaster araneus Bukry (1971)
Discoaster barbadiensis Tan (1927)
Discoaster bifax Bukry (1971)
Discoaster binodosus Martini (1958)
Discoaster cruciformis Martini (1958)
Discoaster deflandrei Bramlette and Riedel (1954)
Discoaster diastypus Bramlette and Sullivan (1961)
Discoaster distinctus Martini (1958)
Discoaster elegans Bramlette and Sullivan (1961)
Discoaster falcatus Bramlette and Sullivan (1961)
Discoaster gemmifer Stradner (1961)
Discoaster germanicus Martini (1958)
Discoaster kuepperi Stradner (1959)
Discoaster lenticularis Bramlette and Sullivan (1961)
Discoaster limbatus Bramlette and Sullivan (1961)
Discoaster lodoensis Bramlette and Riedel (1954)
Discoaster mahmoudii Perch-Nielsen (1981)
Discoaster martinii Stradner (1959)
Discoaster mediosus Bramlette and Sullivan (1961)
Discoaster minimus Sullivan (1964)
Discoaster mohleri Bukry and Percival (1971)
Discoaster multiradiatus Bramlette and Riedel (1954)
Discoaster munitus Stradner (1961)
Discoaster nonaradiatus Klumpp (1953)
Discoaster robustus Haq (1969)
Discoaster saipanensis Bramlette and Riedel (1954)
Discoaster salisburgensis Stradner (1961)
Discoaster septemradiatus (Klumpp, 1953) Martini (1958)
Discoaster strictus Stradner (1961)
Discoaster sublodoensis Bramlette and Sullivan (1961)
Discoaster tanii Bramlette and Riedel (1954)
Discoaster wemmelensis Achuthan and Stradner (1969)
Girgisia gammation (Bramlette and Sullivan, 1961) Varol (1989)

Helicosphaera lophota Bramlette and Sullivan (1961)
Helicosphaera seminulum Bramlette and Sullivan (1961)
Lanternithus minutus Stradner (1962)
Markalius inversus (Deflandré in Deflandré and Fert, 1954) Bramlette and Martini (1964)
Micrantholithus crenulatus Bramlette and Sullivan (1961)
Micrantholithus entaster Bramlette and Sullivan (1961)
Micrantholithus flos Deflandré in Deflandré and Fert (1954)
Nannotetrina cristata (Martini, 1958) Perch-Nielsen (1971)
Nannotetrina fulgens (Stradner, 1960) Achuthan and Stradner (1969)
Neochiastozygus rosenkrantzii Perch-Nielsen (1971)
Neococcolithes dubius (Deflandré, 1954) Black (1967)
Neococcolithes minutus (Perch-Nielsen, 1967) Perch-Nielsen (1971)
Neococcolithes nudus Perch-Nielsen (1971)
Neococcolithes protenus (Bramlette and Sullivan, 1961) Black (1967)
Pontosphaera multipora (Kamptner, 1948) Roth (1970)
Pontosphaera plana (Bramlette and Sullivan, 1961) Haq (1971)
Psuedotriquetrorhabdulus inversus (Bukry and Bramlette, 1969) Wise in Wise and Constans (1976)
Reticulofenestra dictyoda (Deflandré in Deflandré and Fert, 1954) Stradner in Stradner and Edwards (1968)
Reticulofenestra placomorpha (Kamptner, 1948) Stradner in Stradner and Edwards (1968)
Reticulofenestra reticulata (Gartner and Smith, 1967) Roth and Thierstein (1972)
Reticulofenestra reticulata (Hay, Mohler and Wade, 1966) Roth (1970)
Reticulofenestra umbilica (Levin, 1965) Martini and Ritzkowski (1968)
Rhabdosphaera gladius Locker (1967)
Rhabdosphaera inflata Bramlette and Sullivan (1961)
Rhabdosphaera tenuis Bramlette and Sullivan (1961)
Semihololithus kerabyi (Perch-Nielsen, 1971)
Sphenolithus anarrhopus Bukry and Bramlette (1969)
Sphenolithus conicus Bukry (1971)
Sphenolithus conspicuus Martini (1976)
Sphenolithus editus Perch-Nielsen in Perch-Nielsen et al. (1978)
Sphenolithus furcatolithoides Locker (1967)
Sphenolithus moriformis (Bronnimann and Stradner, 1960) Bramlette and Wilcoxon (1967)
Sphenolithus primus Perch-Nielsen (1971)
Sphenolithus radians Deflandré in Grassé (1952)
Sphenolithus spiniger Bukry (1971)

Figure F1. Location map of the Iberia Abyssal Plain showing Leg 173 Sites 1067, 1068, and 1069 (solid triangles). DSDP Site 398 (Leg 47) and ODP Site 900 (Leg 149) are also shown (shaded circles). VdG = Vasco da Gama Seamount; VS = Vigo Seamount; PS = Porto Seamount; ES = Estremadura Spur.

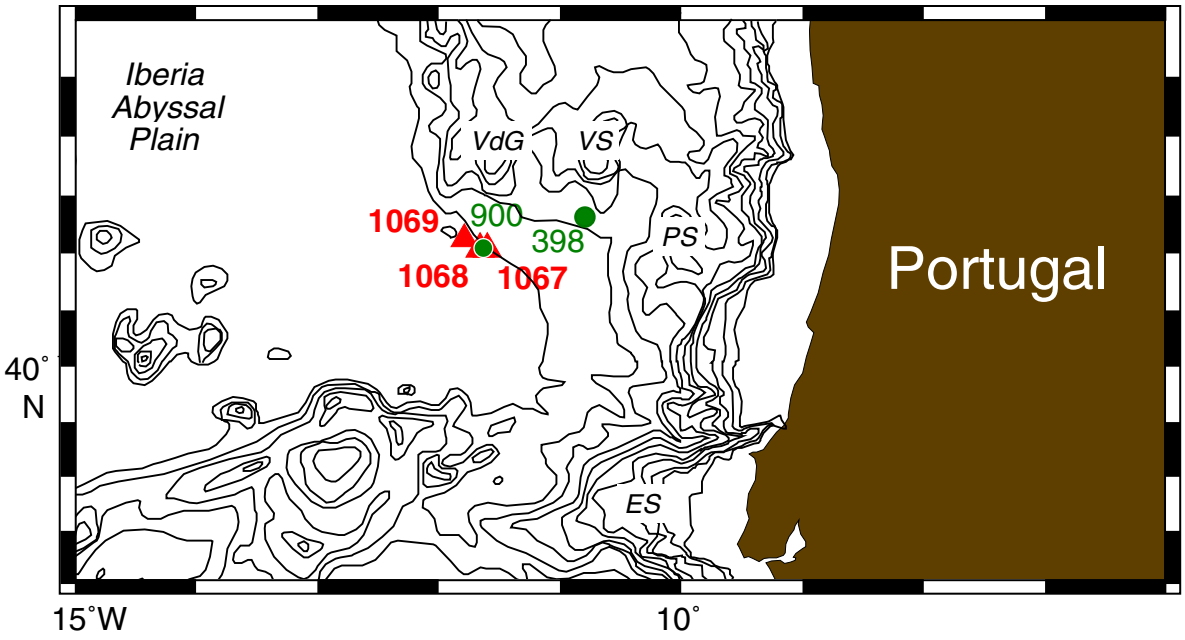

Figure F2. Typical upward-darkening Bouma sequences of calcareous sand/siltstones (Tc), calcareous silty claystones (Td), and calcareous claystones (Te). Notice the increase of moderate brown claystone with depth of section, leading to declining preservation of calcareous nannofossils downhole.

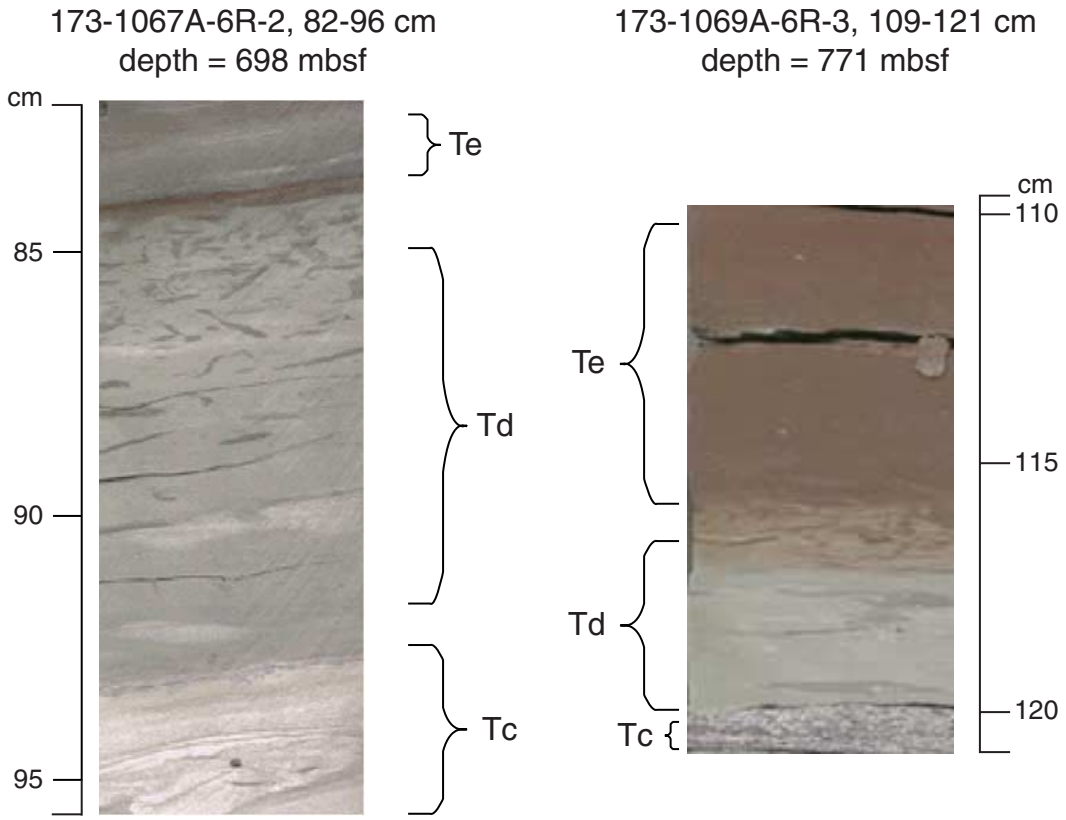

Figure F3. Eocene calcareous nannofossil biostratigraphic datums used in this report after Berggren et al. (1995). Also shown are the zonal units of Okada and Bukry (1980) and Martini (1971).

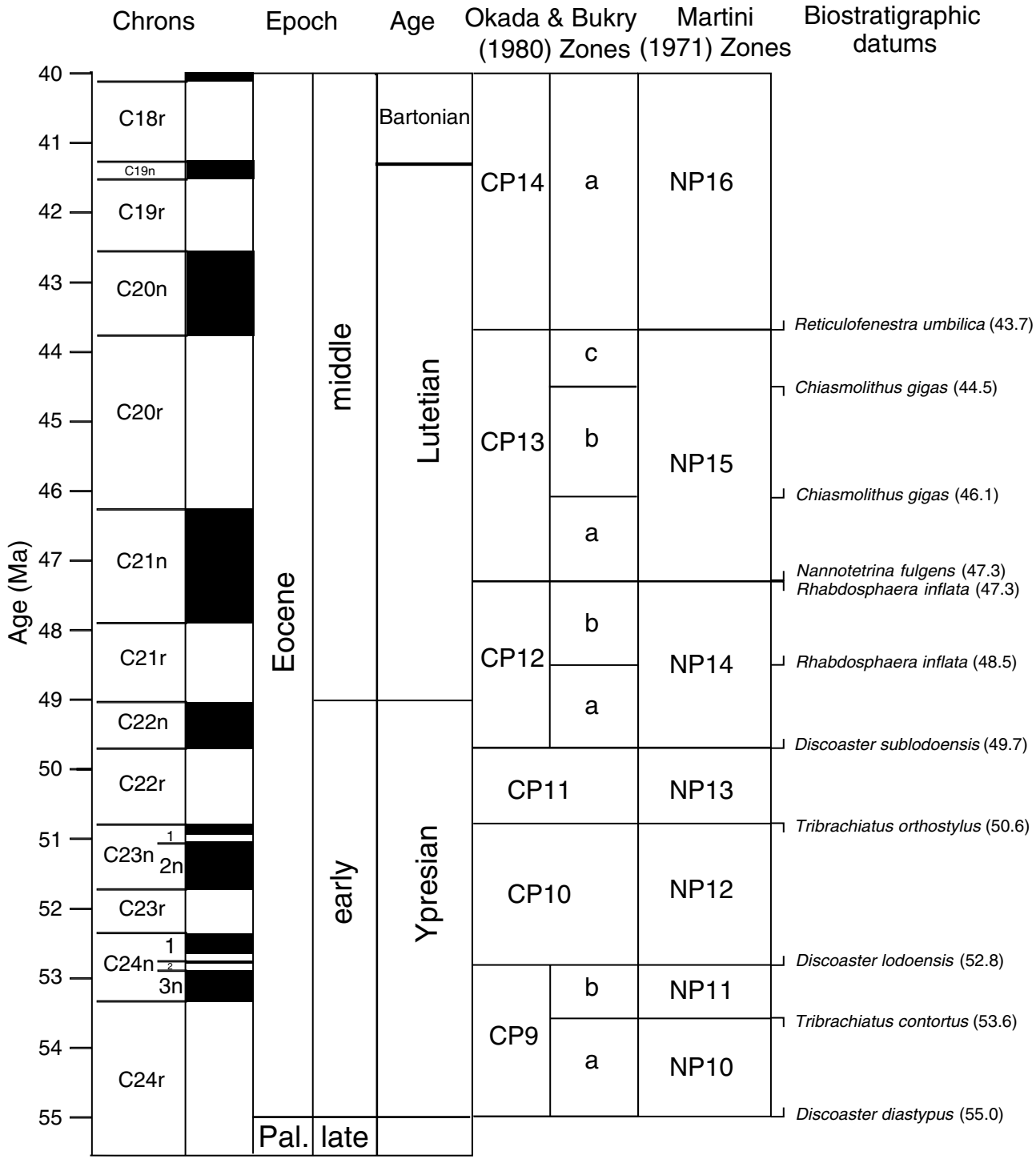

Figure F4. Eocene correlation among holes from Legs 173, 149, and 47B based on calcareous nannofossils. Major biostratigraphic boundaries and events are indicated.

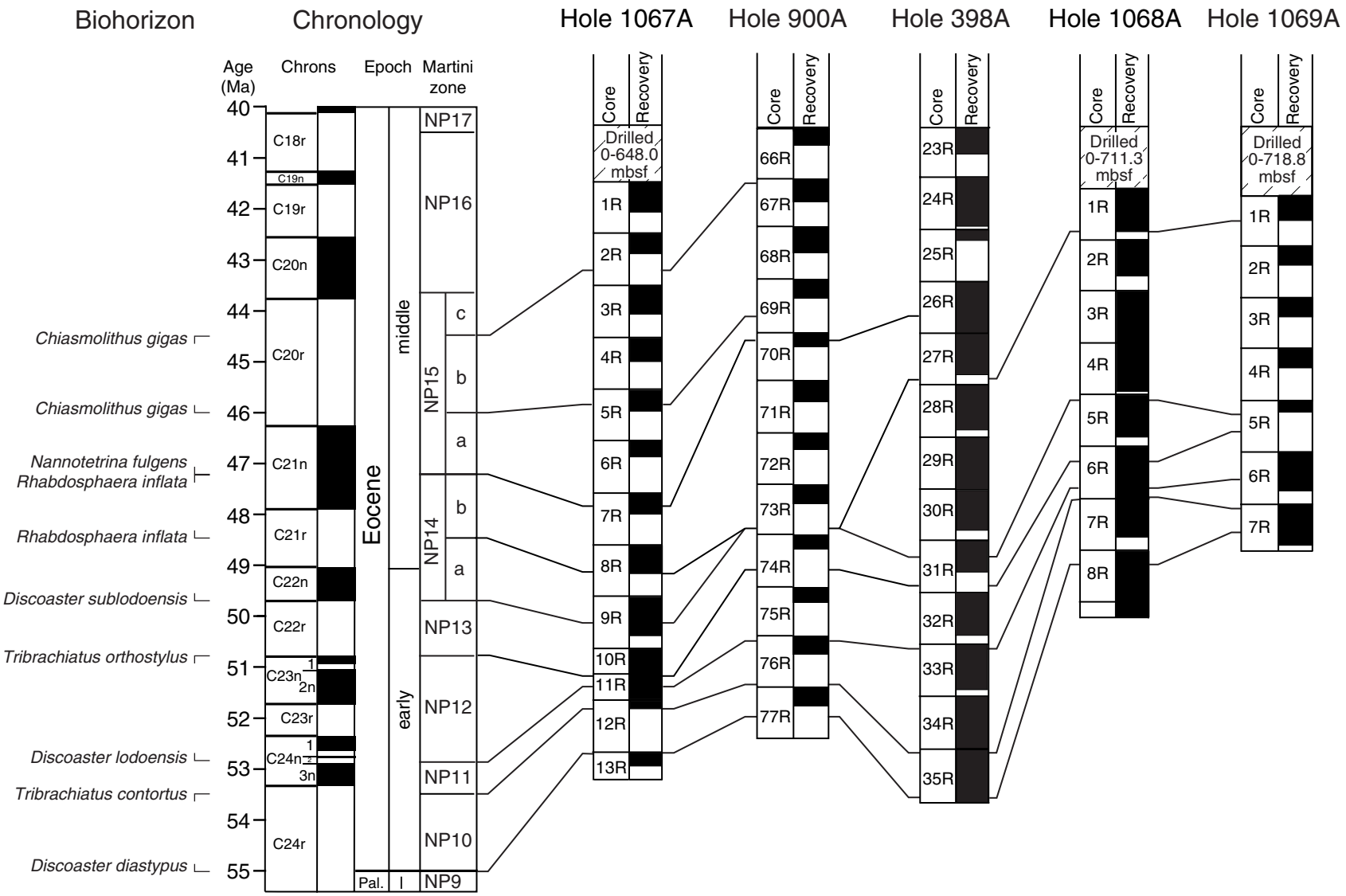

Figure F5. Age-depth plot for Holes 1067A, 1068A, 1069A, 900A, and 398D. Comparison slopes are given in the upper right corner. Pairs of opposed triangles indicate the thickness range of each nannofossil datum. See Tables T2, p. 22, T4, p. 24, T6, p. 26, T7, p. 27, and T8, p. 28, for datums used.

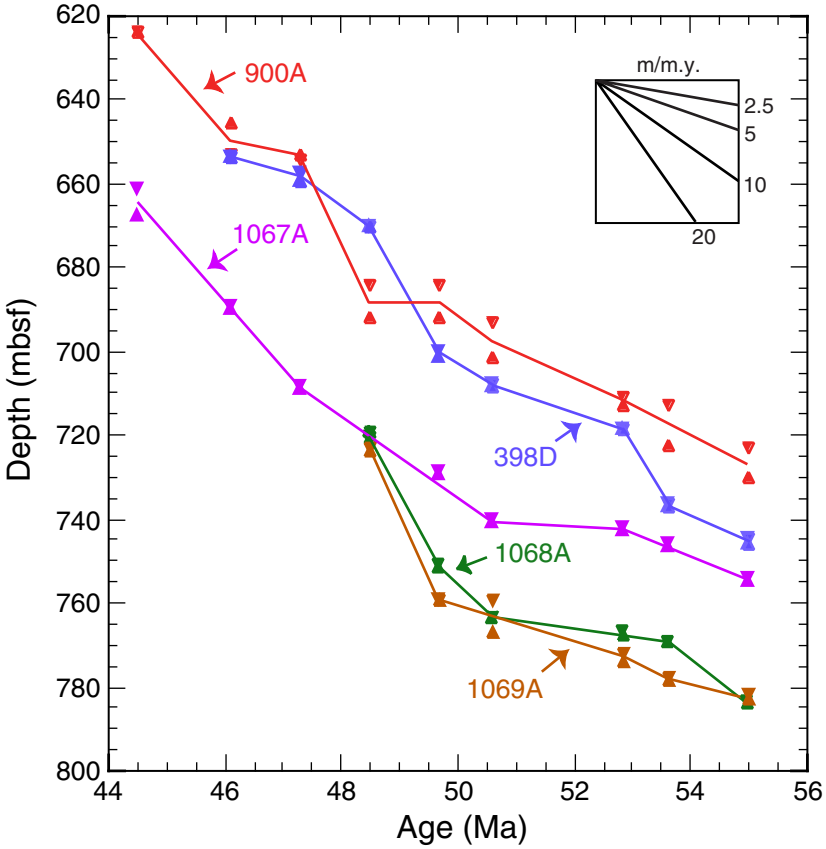

Figure F6. Mass accumulation rates for Holes 1067A, 1068A, 1069A, 900A, and 398D. See Table T9, p. 29, for datums used.

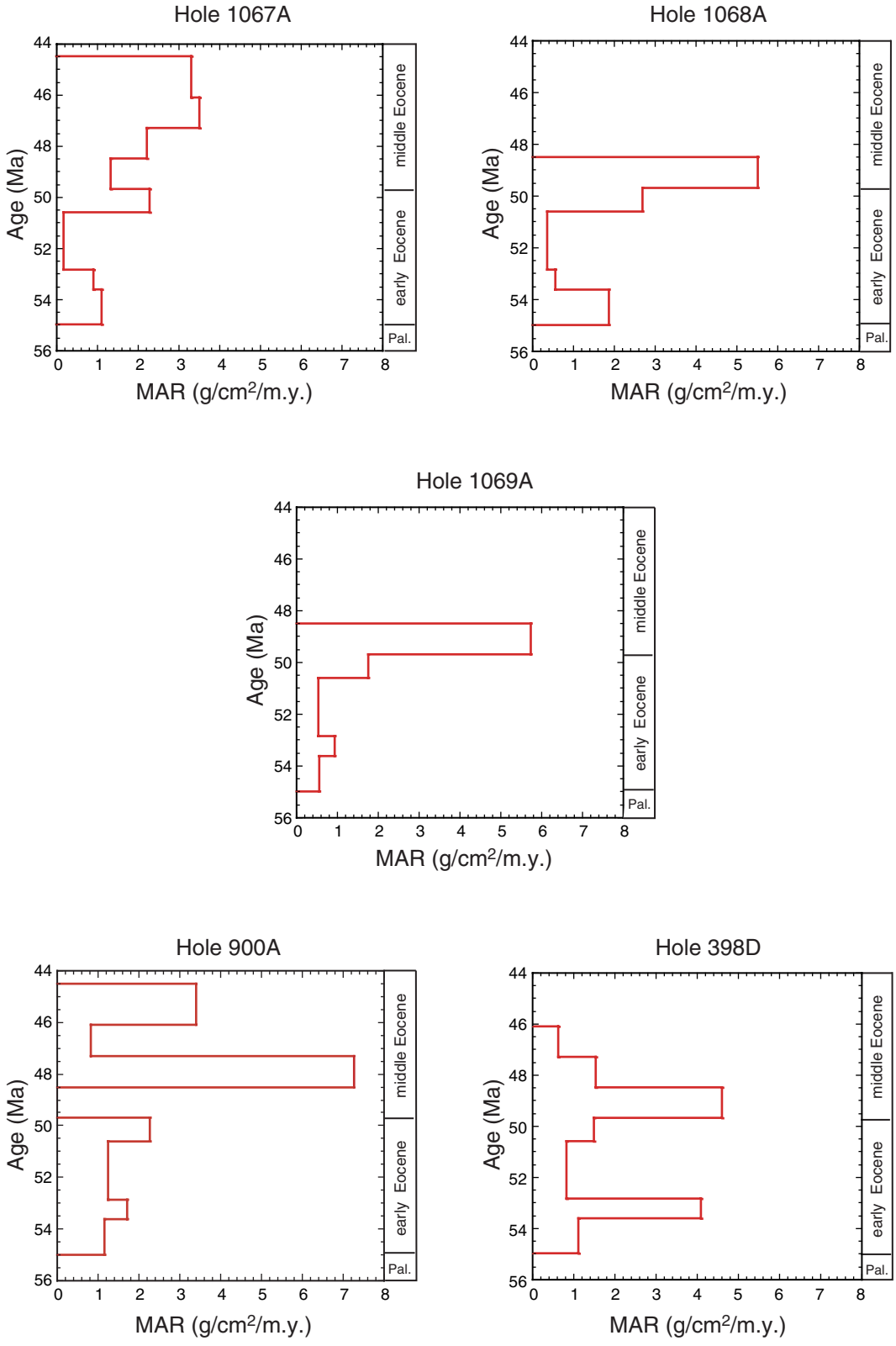

Table T1. Stratigraphic distribution of calcareous nannofossil taxa, Hole 1067A. This table is available in an **oversized format.**

Table T2. Summary of key nannofossil biohorizons, Hole 1067A.

Calcareous nannofossil event	Top core, section, interval (cm)	Bottom core, section, interval (cm)	Depth (mbsf)
	173-1067A-	173-1067A-	
LO *C. gigas*	2R-CC, 13-16	3R-1, 34-35	664.52
FO *C. gigas*	5R-3, 8-9	5R-3, 48-49	689.56
FO *N. fulgens*/LO *R. inflata*	7R-2, 117-118	7R-3, 32-33	708.80
FO *R. inflata*	8R-4, 30-31	8R-CC, 23-25	720.52
FO *D. sublodoensis*	9R-3, 37-38	9R-3, 121-122	728.99
LO *T. orthostylus*	11R-1, 36-37	11R-1, 119-120	740.38
FO *D. lodoensis*	11R-2, 121-222	11R-3, 40-41	742.66
LO *T. contortus*	12R-CC, 10-12	12R-CC, 25-27	746.27
FO *D. diastypus*	13R-1, 30-31	13R-1, 47-48	754.59

Notes: The depth indicated is the average depth between two samples.
LO = last occurrence; FO = first occurrence.

Table T3. Stratigraphic distribution of calcareous nannofossil taxa, Hole 1068A. This table is available in an **oversized format.**

Table T4. Summary of key nannofossil biohorizons, Hole 1068A.

Calcareous nannofossil event	Top core, section, interval (cm)	Bottom core, section, interval (cm)	Depth (mbsf)
	173-1068A-	173-1068A-	
FO *R. inflata*	1R-6, 36-37	1R-CC	719.36
FO *D. sublodoensis*	5R-1, 121-122	5R-2, 35-36	751.43
LO *T. orthostylus*	6R-3, 33-34	6R-3, 121-122	763.37
FO *D. lodoensis*	6R-5, 122-123	6R-6, 123-124	767.58
LO *T. contortus*	6R-CC, 17-19	6R-CC, 23-25	769.50
FO *D. diastypus*	8R-3, 7-8	8R-4, 44-45	782.91

Notes: The depth indicated is the average depth between two samples.
LO = last occurrence; FO = first occurrence.

Table T5. Stratigraphic distribution of calcareous nannofossil taxa, Hole 1069A. This table is available in an **oversized format.**

Table T6. Summary of key nannofossil biohorizons, Hole 1069A.

Calcareous nannofossil event	Top core, section, interval (cm)	Bottom core, section, interval (cm)	Depth (mbsf)
	173-1069A-	173-1069A-	
FO *R. inflata*	1R-4, 0-3	1R-CC	723.31
FO *D. sublodoensis*	5R-2, 29-30	5R-CC, 1-2	759.31
LO *T. orthostylus*	6R-1, 4-5	6R-1, 124-127	767.74
FO *D. lodoensis*	6R-4, 45-47	6R-5, 87-88	773.01
LO *T. contortus*	7R-1, 123-124	7R-1, 147-150	778.15
FO *D. diastypus*	7R-4, 61-63	7R-5, 1-3	782.36

Notes: The depth indicated is the average depth between two samples.
LO = last occurrence; FO = first occurrence.

Table T7. Summary of key nannofossil biohorizons, Hole 900A.

Calcareous nannofossil event	Top core, section, interval (cm)	Bottom core, section, interval (cm)	Depth (mbsf)
	149-900A-	149-900A-	
LO *C. gigas*	66R-CC	67R-1, 36-37	624.00
FO *C. gigas*	69R-2, 107-108	70R-1, 11-12	649.20
FO *N. fulgens*/LO *R. inflata*	70R-1, 11-12	70R-2, 48-49	653.70
FO *R. inflata*	73R-2, 106-107	74R-1, 38-39	688.00
FO *D. sublodoensis*	73R-2, 106-107	74R-1, 38-39	688.00
LO *T. orthostylus*	74R, 46-47	75R-1, 56-57	697.50
FO *D. lodoensis*	76R-1, 24-25	76R-2, 105-106	711.80
LO *T. contortus*	76R-2, 105-106	77R-2, 120-121	717.80
FO *D. diastypus*	77R-3, 3-4	78R-1, 30-31	726.50

Notes: The depth indicated is the average depth between two samples.
LO = last occurrence; FO = first occurrence.

Table T8. Summary of key nannofossil biohorizons, Hole 398D.

Calcareous nannofossil event	Top core, section, interval (cm)	Bottom core, section, interval (cm)	Depth (mbsf)
	47B-398D-	47B-398D-	
FO *R. umbilica*	23R-1, 25-26	23R-2, 60-61	623.70
FO *N. fulgens*	26R-5, 50-51	26R-6, 109-110	658.50
FO *R. inflata*	27R-CC	28R-1, 24-25	670.10
FO *D. sublodoensis*	31R-2, 34-35	31R-3, 24-25	701.00
LO *T. orthostylus*	31R-CC	32R-1, 7-8	708.40
FO *D. lodoensis*	33R-1, 107-108	33R-1, 119-120	718.60
LO *T. contortus*	34R-CC	35R-1, 66-67	736.80
FO *D. diastypus*	35R-6, 80-81	35R-7, 30-31	745.30

Notes: The depth indicated is the average depth between two samples.
LO = last occurrence; FO = first occurrence.

Table T9. Physical properties average values used to calculate mass accumulation rates for Holes 1067A, 1068A, 1069A, 900A, and 398D.

Nannofossil zone/subzone (Okada and Bukry [1980])	Thickness (cm)	Wet bulk density (g/cm^3)	Porosity (%)	Water density (g/gm^3)	Time (k.y.)	MAR ($g/cm^2/k.y.$)
Hole 1067A						
CP13b	2504.5	2.35	21.80	1.03	1600	3.3
CP13a	1923.5	2.40	20.25	1.03	1200	3.5
CP12b	1172.0	2.44	14.67	1.03	1200	2.2
CP12a	847.5	2.21	30.00	1.03	1200	1.3
CP11	1138.5	2.17	34.50	1.03	900	2.3
CP10	228.0	2.09	34.50	1.03	2250	0.2
CP9b	361.0	2.19	27.00	1.03	750	0.9
CP9a	832.0	2.18	31.00	1.03	1400	1.1
Hole 1068A						
CP12a	3220.0	2.30	23.73	1.03	1200	5.5
CP11	1206.0	2.27	25.20	1.03	900	2.7
CP10	367.0	2.36	20.83	1.03	2250	0.4
CP9b	205.0	2.25	24.06	1.03	750	0.5
CP9a	1431.0	2.15	31.93	1.03	1400	1.9
Hole 1069A						
CP12a	3580.0	2.22	28.73	1.03	1200	5.7
CP11	772.0	2.29	24.27	1.03	900	1.7
CP10	683.0	2.12	32.23	1.03	2250	0.5
CP9b	430.0	2.03	38.00	1.03	750	0.9
CP9a	454.0	2.07	36.97	1.03	1400	0.5
Hole 900A						
CP13b	2526.0	2.38	21.80	1.03	1600	3.4
CP13a	450.5	2.37	20.25	1.03	1200	0.8
CP12b	3427.5	2.69	14.67	1.03	1200	7.3
CP12a	0.0	2.47	30.00	1.03	1200	0.0
CP11	949.0	2.50	34.50	1.03	900	2.3
CP10	1433.5	2.30	34.50	1.03	2250	1.2
CP9b	598.0	2.44	27.00	1.03	750	1.7
CP9a	869.0	2.18	31.00	1.03	1400	1.2
Hole 398D						
CP13a	484.5	1.91	45.79	1.03	1200	0.6
CP12b	1157.5	1.97	42.27	1.03	1200	1.5
CP12a	3092.0	2.11	33.40	1.03	1200	4.6
CP11	731.0	2.12	32.41	1.03	900	1.5
CP10	1028.0	2.07	36.24	1.03	2250	0.8
CP9b	1820.0	2.05	37.43	1.03	750	4.0
CP9a	847.0	2.11	33.91	1.03	1400	1.1

Notes: MAR = mass accumulation rate. Physical properties data was compiled by the Shipboard Scientific Parties of Legs 173 (1998c), 149 (1994), and 47B (Williams and Mountain, 1979).

Plate P1. 1. *Nannotetrina fulgens,* Sample 173-1067A-1R-CC, SEM 5500×. **2.** *N. fulgens,* Sample 173-1067A-1R-CC, Ph 1800×. **3.** *N. fulgens,* Sample 173-1067A-1R-CC, XP. **4.** *N. fulgens,* Sample 173-1067A-1R-CC, Pl 2200×. **5.** *N. fulgens,* Sample 173-1067A-1R-CC, Ph. **6.** *N. fulgens,* Sample 173-1067A-1R-CC, XP. **7.** *Nannotetrina cristata,* Sample 173-1068A-5R-CC, Ph 1500×. **8.** *Chiasmolithus solitus,* Sample 173-1067A-1R-CC, 21–23 cm, Ph 1800×. **9.** *C. solitus,* Sample 173-1067A-1R-CC, 21–23 cm, XP. SEM = scanning electron micrography. Light micrography: XP = cross-polarized light; Ph = phase-contrast light; Pl = parallel light. (**Plate shown on next page.**)

Plate P1 (continued). (Caption on previous page.)

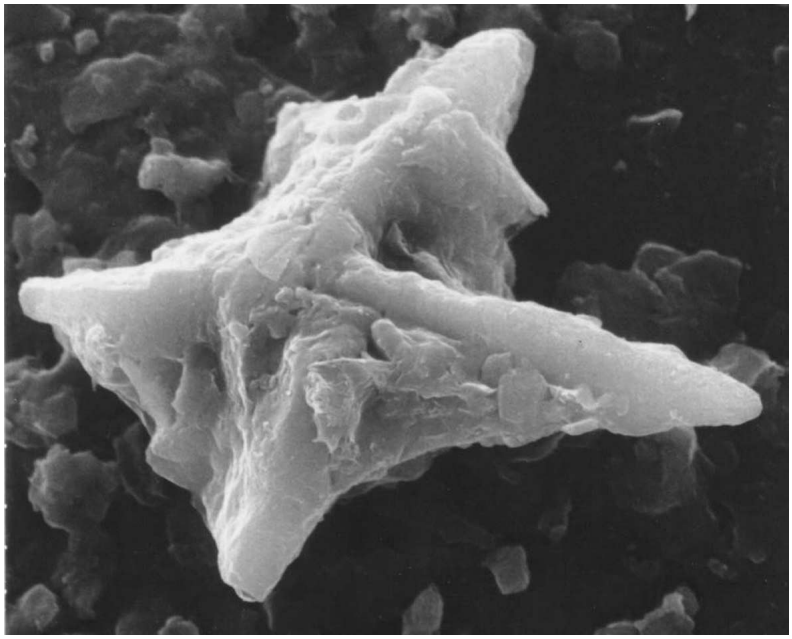
1

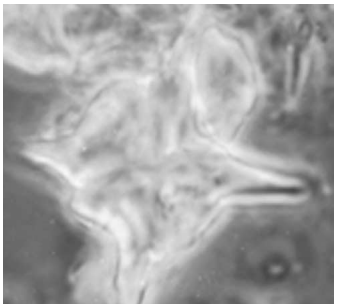
2

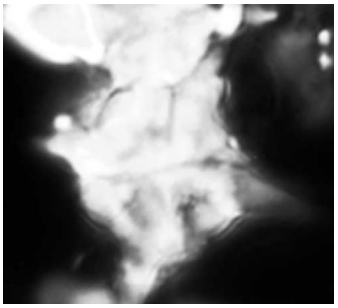
3

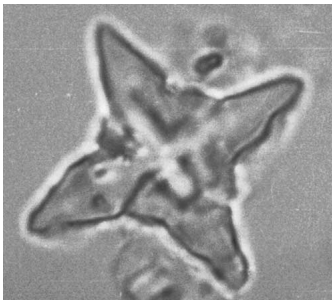
4

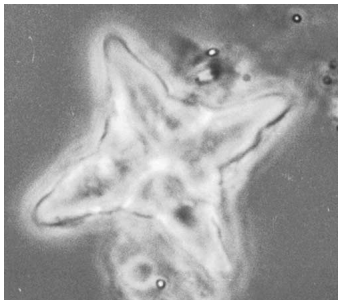
5

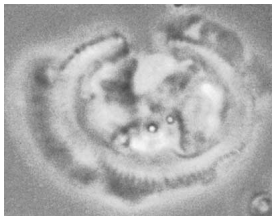
8

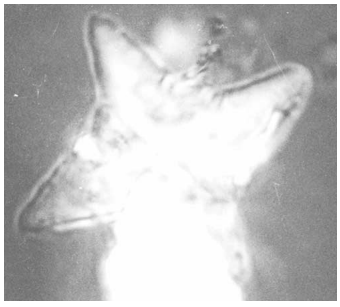
6

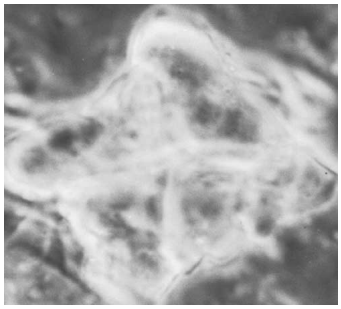
7

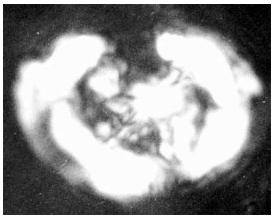
9

Plate P2. 1. *Coccolithus pelagicus,* Sample 173-1067A-1R-CC, 21–23 cm, SEM 5000×. **2.** *Reticulofenestra placomorpha,* Sample 173-1067A-2R-3, 34–35 cm, Ph 2900×. **3.** *R. placomorpha,* Sample 173-1067A-2R-3, 34–35 cm, XP. **4.** *Chiasmolithus gigas,* Sample 173-1067A-3R-2, 13–14 cm, Ph 2300×. **5.** *C. gigas,* Sample 173-1067A-3R-2, 13–14 cm, XP. **6.** *C. gigas,* Sample 173-1067A-1R-CC, 21–23 cm, SEM 6000×. **7.** *Braarudosphaera discula,* Sample 173-1067A-1R-CC, 21–23 cm, Ph 2900×. **8.** *B. discula,* Sample 173-1067A-1R-CC, 21–23 cm, XP. **9.** *Semihololithus keryabi*, Sample 173-1067A-1R-3, 36–37 cm, Ph 2900×. **10.** *S. keryabi*, Sample 173-1067A-1R-3, 36–37 cm, XP. **11.** *Campylosphaera dela,* Sample 173-1068A-4R-2, 36–37 cm, Ph 3500×. **12.** *C. dela,* Sample 173-1068A-4R-2, 36–37 cm, XP. SEM = scanning electron micrography. Light micrography: XP = cross-polarized light; Ph = phase-contrast light; Pl = parallel light. (**Plate shown on next page.**)

Plate P2 (continued). (Caption on previous page.)

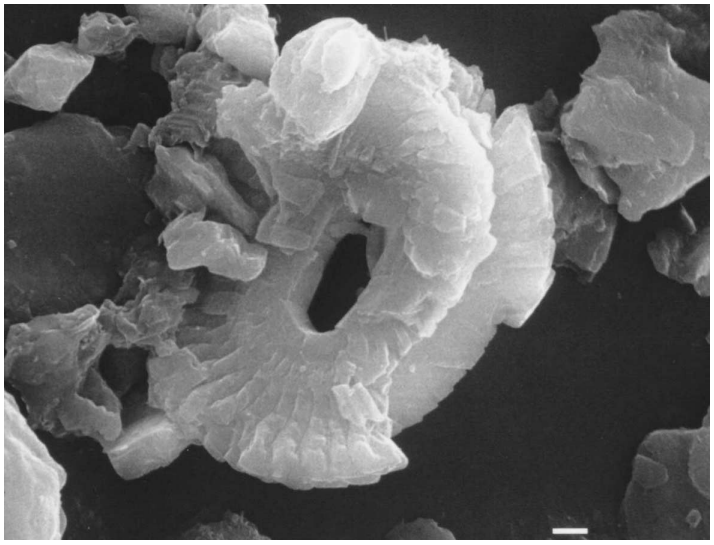
1

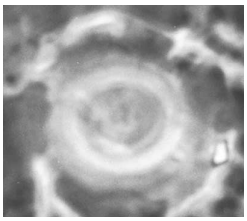
2

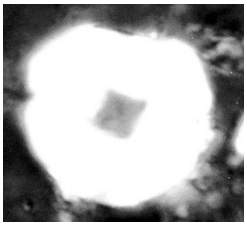
3

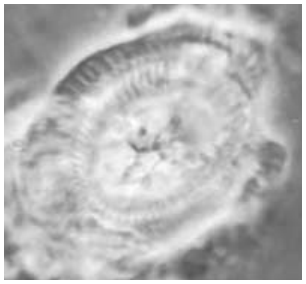
4

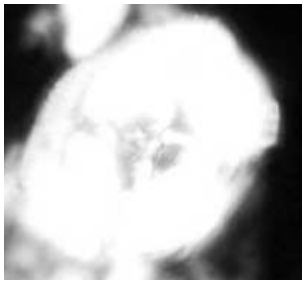
5

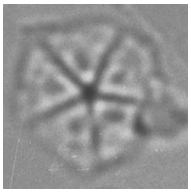
7

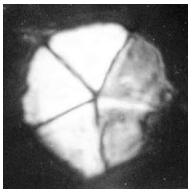
8

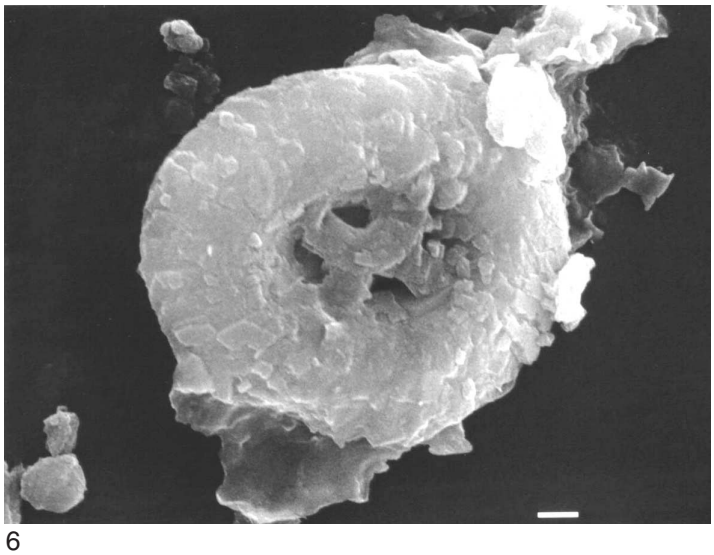
6

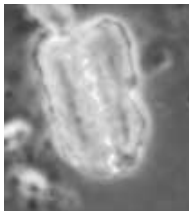
9


10

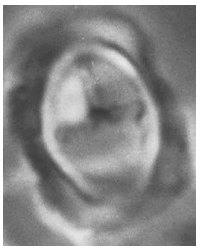
11


12

Plate P3. 1. *Discoaster deflandrei* and *Coccolithus pelagicus,* Sample 173-1067A-1R-CC, 21–23 cm, SEM 7000×. **2.** *Discoaster gemmifer,* Sample 173-1068A-4R-2, 102–103 cm, Ph 1300×. **3.** *Discoaster binodosus,* Sample 173-1068A-6R-3, 121–123 cm, SEM 9500×. **4.** *Discoaster lodoensis,* Sample 173-1067A-9R-4, 119–120 cm, Ph 1800×. **5.** *Tribrachiatus orthostylus,* Sample 173-1067A-11R-2, 121–122 cm, Ph 1900×. **6.** *Discoaster* sp., Sample 173-1067A-1R-CC, 21–23 cm, SEM 9500×. **7.** *Tribrachiatus contortus,* Sample 173-1068A-7R-5, 75–77 cm, Ph 1400×. **8.** *T. contortus,* Sample 173-1068A-7R-5, 75–77 cm, XP. **9.** *Tribrachiatus bramlettei,* Sample 173-1069A-6R-CC, Ph 1300×. **10.** *T. bramlettei,* Sample 173-1069A-6R-CC, XP. **11.** *Discoaster kuepperi,* Sample 173-1067A-9R-4, 119–120 cm, Ph 2100×. **12.** *D. kuepperi,* Sample 173-1067A-9R-4, 119–120 cm, Ph 2100×. **13.** *Rhabdosphaera inflata*, Sample 173-1069A-1R-1, 120–123 cm, XP 1600×. **14.** *R. inflata*, Sample 173-1069A-1R-1, 120–123 cm, XP 1600×. SEM = scanning electron micrography. Light micrography: XP = cross-polarized light; Ph = phase-contrast light; Pl = parallel light. (**Plate shown on next page.**)

Plate P3 (continued). (Caption on previous page.)

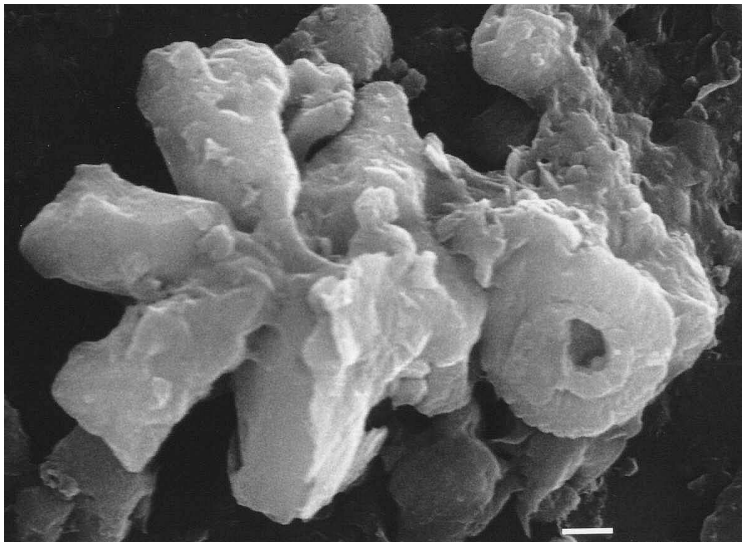
1

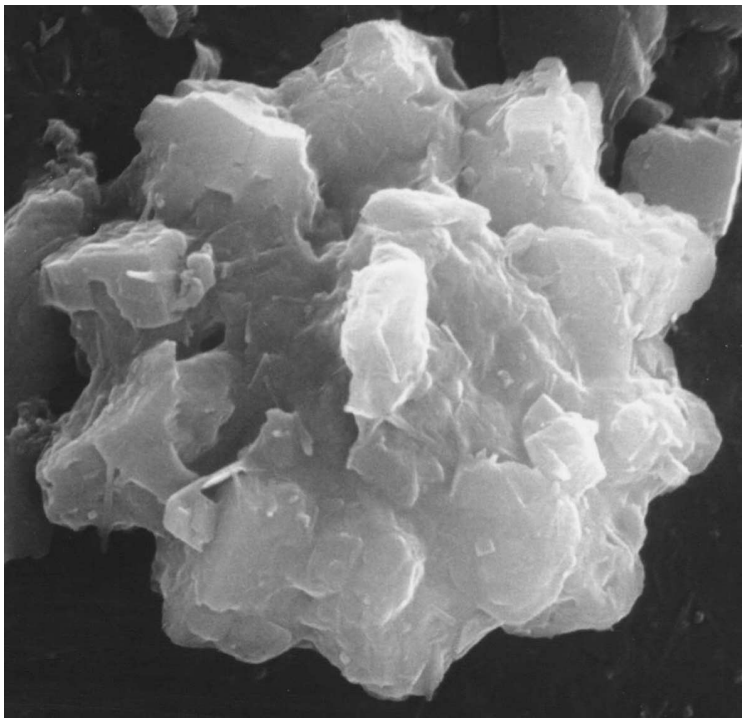
6

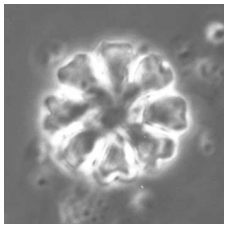
2

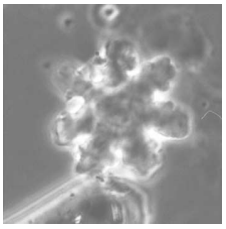
3

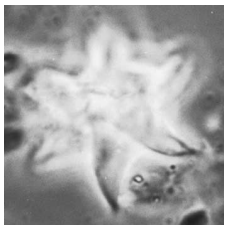
4

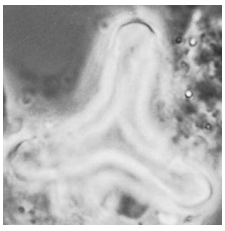
5

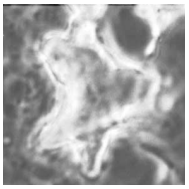
7

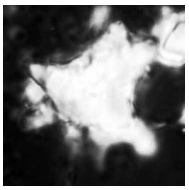
8

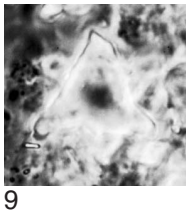
9

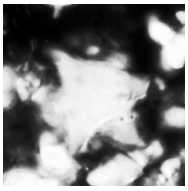
10

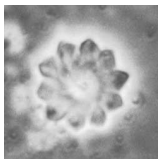
11


12

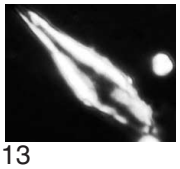
13


14